The fine-scale structure of the global tropopause derived from COSMIC GPS radio occultation measurements

Seok-Woo Son,[1] Neil F. Tandon,[2] and Lorenzo M. Polvani[2,3]

[1]   The spatiotemporal structure of the lapse-rate tropopause is examined by using state-of-the-art Global Positioning System radio occultation measurements from the Constellation Observing System for Meteorology, Ionosphere and Climate (COSMIC) Formosa Satellite Mission 3 mission. The high temporal and spatial resolutions of the data reveal the detailed structure of tropopause properties such as pressure (p_t), temperature (T_t), and sharpness (N_t^2) and their relationships to upper tropospheric and lower stratospheric processes. The overall results are generally in good agreement with previous studies. The climatology of all three tropopause properties shows largely homogeneous structure in the zonal direction: noticeable asymmetries are found only in the tropics and the Northern Hemisphere extratropics during boreal winter owing to localized tropospheric processes. This contrasts with the seasonal cycles of tropopause properties which are significantly influenced by stratospheric processes such as the Brewer-Dobson circulation, the polar vortex, and the radiative processes near the tropopause. On intraseasonal time scales, p_t and T_t exhibit significant variability over the Asian summer monsoon and the subtropics where double tropopauses frequently occur. In contrast, N_t^2 shows maximum variability in the tropics where p_t and T_t have minimum variability, possibly a consequence of vertically propagating waves. The tropopause properties derived from COSMIC observations are further applied to evaluate tropopause data directly available from the NCEP-NCAR Reanalysis (NNR). Although the NNR tropopause data have been widely used in climate studies, they are found to have significant and systematic biases, especially in the subtropics. This suggests that the NNR tropopause data should be treated with great caution in any quantitative studies.

Citation: Son, S.-W., N. F. Tandon, and L. M. Polvani (2011), The fine-scale structure of the global tropopause derived from COSMIC GPS radio occultation measurements, *J. Geophys. Res.*, *116*, D20113, doi:10.1029/2011JD016030.

1. Introduction

[2]   The tropopause has often been examined to better understand stratosphere-troposphere exchange and coupling. Its properties are known to characterize the cross-tropopause transport of moisture and chemical constituents. For instance, the amount of moisture transported from the tropical troposphere into the stratosphere is primarily controlled by the cold-point temperature in the deep tropics [*Mote et al.*, 1996] (more recently, *Fueglistaler et al.* [2009]). The exchange of chemical tracers across the extratropical tropopause is also known to be sensitive to the temperature and stratification at the tropopause [*Holton et al.*, 1995; *Butchart and Scaife*, 2001; *Kunz et al.*, 2009]. Since small changes in tracer distributions

in the upper troposphere and lower stratosphere (UTLS) could drive significant changes in the troposphere by modifying the radiative budget, a precise understanding of tropopause properties is therefore important.

[3]   The tropopause has recently received much attention because of its promise as an indicator of climate change. *Santer et al.* [2003a] and *Son et al.* [2009] have shown that long-term change of the global tropopause is a useful "fingerprint" of global climate change. Due to anthropogenic warming and stratospheric ozone depletion, global tropopause pressure (height) has been decreasing (increasing) during the last four decades. It is also known that the long-term trend of extratropical tropopause pressure is linked to changes in the tropospheric circulation, in particular the Hadley cell [e.g., *Lu et al.*, 2007] and the westerly jet [e.g., *Lorenz and DeWeaver*, 2007]. Both observations and climate model simulations have shown that the recent decrease in extratropical tropopause pressure is associated with a poleward expansion of the Hadley cell and a poleward displacement of the westerly jet in both hemispheres. *Seidel and Randel* [2007] have further demonstrated that the location of the subtropical tropopause, more specifically the location of peak double tropopause frequency in the subtropics,

[1]Department of Atmospheric and Oceanic Sciences, McGill University, Montreal, Quebec, Canada.
[2]Department of Applied Physics and Applied Mathematics, Columbia University, New York, New York, USA.
[3]Department of Earth and Environmental Sciences, Columbia University, New York, New York, USA.

is a useful measure of the poleward extent of the tropical belt. These studies suggest that a quantitative characterization of the global tropopause is important in improving our understanding not only of physical processes in the UTLS, but also of the large-scale circulation in the troposphere and its long-term change.

[4] The spatiotemporal structure of the global tropopause has previously been examined with radiosonde data. It is well known that tropopause height reaches its highest altitude in the tropics, drops sharply across the subtropical jet, and settles to lower altitudes in the extratropics. Previous studies, however, have focused mostly on the zonal mean tropopause or the tropopause over limited regions [e.g., *Reid and Gage*, 1996; *Seidel et al.*, 2001]. The latitude-longitude structure of the global tropopause and its variability have rarely been examined, because of the limited spatial coverage of radiosonde observations. Although *Seidel et al.* [2001] attempted a spatial characterization of the tropical tropopause, only a crude picture emerges due to sparse data and heavy interpolation.

[5] As an alternative data source, reanalysis products have been widely used [*Hoerling et al.*, 1991; *Hoinka*, 1998, 1999; *Highwood et al.*, 2000; *Zängl and Hoinka*, 2001]. The quality of the data, however, has been questionable. For example, *Santer et al.* [2003b] have shown that the climatology and temporal evolution of the zonal mean tropopause properties derived from the two major reanalysis data sets, the European Centre for Medium-Range Weather Forecasts (ECMWF) 40 Year Re-analysis (ERA-40) and the National Centers for Environmental Protection–National Center for Atmospheric Research (NCEP-NCAR) Reanalysis (NNR), have considerable differences even in the postsatellite era. In addition, coarse vertical resolution of reanalysis data makes them ill suited for analyzing the sharpness of the tropopause [*Birner et al.*, 2006].

[6] A significant advance has recently come from the Global Positioning System (GPS) radio occultation (RO) observations. The GPS RO systems provide remarkably accurate temperature measurements in the UTLS with typical error of less than 1 K [e.g., *He et al.*, 2009], with the capability of global coverage. The first such system was the GPS Meteorology (GPS/MET) mission, which took place between 1995 and 1997. Its measurements, however, were reliable only at altitudes higher than 10 km, making it suitable for studying only the tropical tropopause [*Randel et al.*, 2003]. Observations of the global tropopause became possible later with the Challenging Minisatellite Payload (CHAMP) and Satélite de Aplicaciones Científicas-C (SAC-C) missions, which were launched in 2000. *Kishore et al.* [2006] have shown that the 1 year tropopause climatologies from these two missions are essentially the same. Using multiyear CHAMP and SAC-C data, *Schmidt et al.* [2005] have analyzed the climatology and subseasonal variability of global tropopause properties. *Randel et al.* [2007a] and *Grise et al.* [2010] have also used CHAMP data to characterize tropopause sharpness. These studies have revealed tropopause structure in regions that were previously accessible only via reanalysis data.

[7] While the CHAMP and SAC-C missions have substantially improved our understanding of the tropopause, their spatial coverage is still relatively coarse, as they rely on a single low-orbiting satellite for receiving GPS radio signals. Much-improved spatial coverage has very recently become

available from the Constellation Observing System for Meteorology, Ionosphere and Climate (COSMIC) Formosa Satellite Mission 3 mission [*Anthes et al.*, 2008]. This mission was launched in 2006 jointly by the National Aeronautics and Space Administration and Taiwan's National Space Organization. The occultation system uses six low-orbiting satellites, providing spatial coverage of about 2000 soundings per day, evenly spread over the globe. This is about an order of magnitude higher spatial coverage than the CHAMP and SAC-C missions.

[8] The primary goal of this study is to examine the spatiotemporal structure of the global tropopause using high-resolution COSMIC data. By extending and updating earlier studies, especially those based on the previous GPS RO missions, we provide a more comprehensive view of the global tropopause. As in previous studies, we focus on three tropopause properties: lapse-rate tropopause pressure (p_t), temperature (T_t) and sharpness (N_t^2). The climatology, seasonal cycle and intraseasonal variability of these properties are extensively examined, and possible physical processes responsible for their morphology are discussed.

[9] The results are then applied to evaluate the quality of the NNR tropopause data. Although it is known that the thermal tropopause properties calculated from analysis data are reasonably accurate [e.g., *Schmidt et al.*, 2005], the quality of p_t and T_t data directly available from NNR has been questionable. *Birner* [2010a], for instance, showed that daily p_t data from NNR may have a serious bias in the subtropics because of the inaccurate tropopause definition and detection algorithm used in NNR. In this study, the bias of NNR tropopause data is quantitatively evaluated by using COSMIC observations.

[10] This paper is organized as follows. Section 2 describes data sources and analysis methods. Definition of each tropopause property is also provided. In section 3, we present the climatology of the three tropopause properties, followed by their seasonal cycle and intraseasonal variability. In section 4 the overall results are compared with NNR tropopause data. Section 5 provides a summary and conclusion.

2. Data and Methods

2.1. Data

[11] The primary data sets used in this study are the temperature profiles derived from the COSMIC mission [*Anthes et al.*, 2008]. Dry temperature profiles, archived at the COSMIC Data Access and Archival Center, are analyzed for the time period spanning September 2006 to August 2009 (3 years).

[12] Individual temperature profiles, which have variable vertical resolution, are linearly interpolated to a standard 200 m vertical grid in accordance with the approximate physical resolution of GPS RO measurements [*Kursinski et al.*, 2000; *Schmidt et al.*, 2005]. Tropopause properties are computed from this interpolated data, and then sorted into 5° latitude by 5° longitude bins to generate spatial maps. No interpolation is applied. In Figure 1, the total number of available soundings in each grid box is shown for December-January-February (DJF) and June-July-August (JJA). Although the spatial coverage is relatively coarse in the deep tropics and the polar regions, it is largely homogeneous and
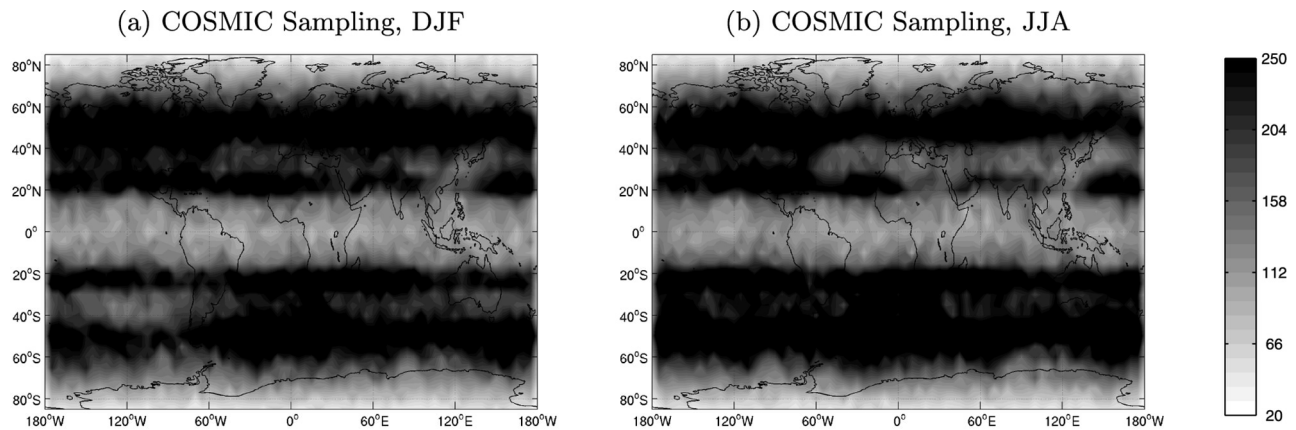
(a) COSMIC Sampling, DJF (b) COSMIC Sampling, JJA

Figure 1. Number of soundings of COSMIC GPS RO measurements between September 2006 and August 2009 for (a) DJF and (b) JJA. The number of soundings is calculated for each 5° longitude by 5° latitude bin.

reasonably dense in the midlatitudes between 20° and 70° (about 0.8 soundings per day per grid box).

[13] For comparison, tropopause data from radiosondes are also examined. They are obtained from the Integrated Global Radiosonde Archive [*Durre et al.*, 2006] for the same time period as COSMIC observations. Following *Seidel and Randel* [2006], both 00:00 UTC and 12:00 UTC data are used for the stations which have homogeneous observations in time. In order to examine the possible physical processes influencing tropopause properties, NNR [*Kalnay et al.*, 1996] and National Oceanic and Atmospheric Administration Outgoing Long-wave Radiation (OLR) data [*Liebmann and Smith*, 1996] are also analyzed for the same time period as COSMIC data. For these fields, monthly mean data are used. However, comparison of NNR tropopause data with COSMIC observations is performed with twice-daily data.

2.2. Tropopause Properties

[14] In this study, we use the thermal definition of the tropopause, often referred to as the "lapse-rate" tropopause. Although the cold-point tropopause has also been widely used, it is not considered here as it is physically meaningful only in the tropics. The characteristics of the tropical cold-point tropopause will be reported in a separate paper. Following the *World Meteorological Organization* (WMO) [1957], the tropopause is defined as "the lowest level at which the lapse-rate decreases to 2°C/km or less, provided that the average lapse-rate between this level and all higher levels within 2 km does not exceed 2°C/km." It is detected using the algorithm employed by *Schmidt et al.* [2005] except for a minimum tropopause height. The bottommost level is set to 5 km at the pole and is increased to 10 km at the equator according to the relation $7.5 + 2.5 \cos(2\varphi)$, where φ is the latitude. This empirical constraint is applied to avoid noise caused by water vapor in the lower troposphere [*Anthes et al.*, 2008].

[15] While tropopause pressure (p_t) and temperature (T_t) are directly determined, the sharpness of the tropopause (N_t^2) requires an additional computation. In this study, N_t^2 is defined by the static stability change across the tropopause:

$$N_t^2 = N_{LS}^2 - N_{UT}^2 \approx \frac{g}{T_t}(\gamma_{UT} - \gamma_{LS}), \quad (1)$$

where N^2, γ, and g are the dry static stability, the temperature lapse rate, and the gravitational acceleration, respectively. Subscripts UT and LS denote the upper troposphere (UT) averaged from 0 to 1 km *below* the tropopause and the lower stratosphere (LS) averaged from 0 to 1 km *above* the tropopause, respectively. This metric is similar to the one used by *Schmidt et al.* [2005] which is based on the temperature lapse-rate difference across the tropopause. Note also that N_{LS}^2 represents the strength of the temperature inversion above the tropopause, the so-called tropopause inversion layer (TIL), which has been often used to characterize tropopause sharpness [*Birner et al.*, 2002; *Birner*, 2006; *Grise et al.*, 2010].

3. Results

[16] We start with a very brief review of tropopause theories, for a better understanding of the results presented below. The formation and maintenance mechanisms of p_t and T_t are relatively well understood. The climatological p_t and T_t in the tropics are, to a first order, determined by radiative and convective processes [*Manabe and Strickler*, 1964; *Held*, 1982]. In the extratropics, baroclinic eddies largely set the climatological p_t and T_t [*Held*, 1982; *Lindzen*, 1993; *Schneider*, 2004]. Both the tropical and extratropical tropopause properties are also modified by stratospheric processes such as the Brewer-Dobson circulation and the polar vortices [*Gabriel et al.*, 1999; *Kirk-Davidoff and Lindzen*, 2000; *Thuburn and Craig*, 2000; *Birner*, 2010b]. It is also known that short-term variability of p_t and T_t is primarily controlled by organized deep convection and equatorial waves in the tropics [*Randel et al.*, 2003; *Son and Lee*, 2007; *Ryu et al.*, 2008] and baroclinic eddies in the extratropics [*Zängl and Wirth*, 2002; *Son et al.*, 2007].

[17] The sharpness of the tropopause, N_t^2, is a relatively new subject. It has been often examined in the context of the TIL, whose strength (N_{LS}^2) is qualitatively similar to N_t^2 in both space and time. Observational studies have shown that TIL is sharp in the tropics year-round [*Grise et al.*, 2010] and in the extratropics during the summer [*Birner*, 2006; *Randel et al.*, 2007a; *Grise et al.*, 2010]. Different theories have been proposed for the formation of the extratropical TIL. Using potential vorticity inversion, *Wirth* [2003] has

attributed the midlatitude TIL to synoptic-scale weather systems. He has shown that a sharp temperature inversion forms right above the tropopause at the center of anticyclonic vortices, resulting in strong N_{LS}^2. Although cyclonic vortices do not produce strong N_{LS}^2, the composite of anticyclonic and cyclonic vortices still shows a distinct N_{LS}^2 due to significantly strong N_{LS}^2 in association with anticyclonic vortices. This argument has subsequently been confirmed by *Son and Polvani* [2007] from simple general circulation model integrations, and by *Randel et al.* [2007a] from observations. *Birner* [2010b] proposed that the midlatitude TIL is also affected by the stratospheric circulation. He showed that adiabatic warming in the descending branch of the Brewer-Dobson circulation could enhance the temperature inversion in the LS, strengthening N_{LS}^2 in the midlatitudes. In addition to dynamical considerations, *Randel et al.* [2007a], *Kunz et al.* [2009], and *Randel and Wu* [2010] have proposed that strong N_t^2 in the summer hemisphere high latitudes could result from radiative processes in the UTLS. Observations show a substantial amount of water vapor near the polar tropopause in the summer hemisphere [e.g., *Randel and Wu*, 2010]. The resulting radiative cooling at the tropopause level can generate a sharp temperature inversion layer in the LS (high N_{LS}^2). This radiative process has recently been confirmed by climate model simulations [*Birner*, 2010b].

[18] With the above theoretical background in hand, we next examine the spatiotemporal structure of the global tropopause. The climatology, seasonal cycle and intraseasonal variability of three tropopause properties (p_t, T_t, and N_t^2) are described in detail.

3.1. Climatology

[19] The climatology of each tropopause property is presented in Figures 2a–2c. In general, the overall structure is qualitatively similar to the one obtained from CHAMP [e.g., *Schmidt et al.*, 2005; *Grise et al.*, 2010] and reanalysis data [e.g., *Hoerling et al.*, 1991; *Hoinka*, 1998, 1999]. To ensure the capability of COSMIC observations in tropopause detection, p_t and T_t shown in Figures 2a and 2b are quantitatively compared with radiosonde observations. The climatological differences in p_t and T_t between COSMIC and radiosonde observations are illustrated in Figure 3. They are computed by simply subtracting climatological p_t and T_t of radiosonde observations from those of COSMIC measurements at the nearest grid point. In other words, pointwise radiosonde observations are compared with area-integrated (5° × 5°) COSMIC observations. It is found that the difference is reasonably small in most areas, typically less than a few percent of the climatological value. The seasonal mean and intraseasonal variability also exhibit reasonably small and unorganized differences (not shown). Nonnegligible biases are, however, found around at 30–40° in both hemispheres. These regions largely coincide with the regions where tropopause properties change abruptly with latitude (see Figures 2a–2c), suggesting that higher spatial resolution

is needed there. Although significant differences are also found near the South Pole, these are likely caused by sampling error. As shown in Figure 1, only a limited number of soundings are available at the pole.

[20] Returning to Figure 2, it can be seen that the climatological p_t reaches its minimum (~80 hPa) over the equator and stays homogeneous in latitude within ~20° of the equator. It sharply increases around 35°, settling to values of ~250–300 hPa in the extratropics. A qualitatively similar structure is also evident in T_t (Figure 2b). In contrast to p_t and T_t, N_t^2 shows a very different structure (Figure 2c): although it is inversely correlated with T_t in the tropics (i.e., cooling at the tropopause level would increase γ_{UT} but decrease γ_{LS}, resulting in stronger N_t^2 (equation (1)), there is essentially no correlation in the extratropics. This result suggests that extratropical N_t^2 may be driven by mechanisms different from those maintaining p_t and T_t. We discuss this in section 3.2.

[21] The latitudinal distribution of tropopause properties exhibits an abrupt transition across the subtropical jet (see the subtropical wind speed maxima in Figure 2d). This can be attributed to the occurrence of a double tropopause in this region. *Randel et al.* [2007b], among others, have shown that in the subtropics a double tropopause is often present, i.e., a high (or tropical) tropopause height aligned with the top of the subtropical jet and a low (or extratropical) tropopause height aligned with its bottom. The tropical tropopause is often detectable up to 40–50°, whereas the extratropical tropopause starts to appear around 30°. As described in section 2.2, the *WMO* [1957] definition of the tropopause captures only the first, or lowest, tropopause. Hence, p_t changes abruptly at the lowest latitude where the extratropical tropopause appears.

[22] The subtropical transition however occurs at different latitudes for each tropopause property. For instance, the maximum T_t gradient is found about 5–10° equatorward of the maximum p_t gradient (compare Figures 2a and 2b). This difference results from the temperature distribution in the UTLS. Figure 4a illustrates the zonal mean temperature and its latitudinal gradient from the COSMIC observations. The maximum temperature gradient is found on the poleward side of the tropical cold point at ~35°. This is the latitude where the maximum p_t gradient is also found (Figure 4b). Along the tropopause, however, the temperature gradient rapidly decreases as p_t increases with latitude. Thus, the maximum T_t gradient is slightly equatorward of the maximum p_t gradient (Figure 4b). Unlike p_t and T_t, N_t^2 shows a transition at a much lower latitude with minimum N_t^2 at 25–40° in both hemispheres (Figure 2c). These subtropical minima are collocated with the subtropical jet [see also *Grise et al.*, 2010], and likely caused by the fact that the tropopause is not well defined in this region and temperature keeps decreasing with height across the tropopause (e.g., Figure 4a).

[23] Figures 2a–2c also show that the latitudinal distribution of tropopause properties is not symmetric about the equator. In fact, a strong hemispheric difference is present in the extratropics. Unlike in the Northern Hemisphere (NH),

Figure 2. Annual mean (a) tropopause pressure p_t, (b) temperature T_t, and (c) sharpness N_t^2 derived from COSMIC observations. The shading interval is 8.3 hPa for p_t, 1.2 K for T_t, and 0.09 × 10^{-4} s^{-2} for N_t^2. Background flow derived from NNR data is also shown: (d) 300 hPa zonal wind (contours, with 25 m s^{-1} contour thick) and standard deviation of 300 hPa meridional wind (shaded only for local maxima) and (e) 500 hPa geopotential height deviated from the zonal mean (contours) and NOAA OLR (shaded only for local minima).
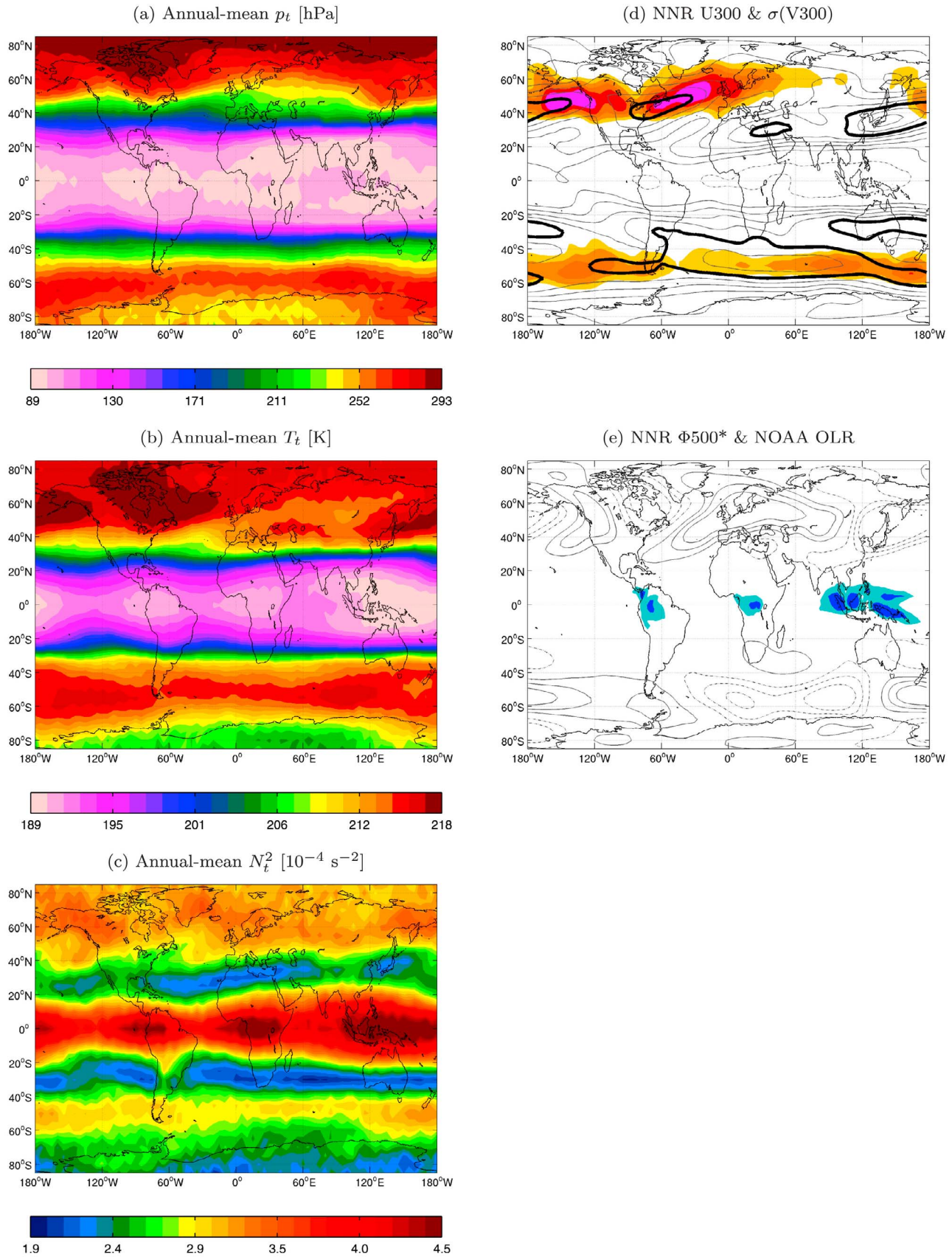
(a) Annual-mean p_t [hPa]

(d) NNR U300 & σ(V300)

(b) Annual-mean T_t [K]

(e) NNR $\Phi500^*$ & NOAA OLR

(c) Annual-mean N_t^2 [10^{-4} s^{-2}]

Figure 2

(a) Radiosonde - COSMIC : Annual-mean p_t [hPa]

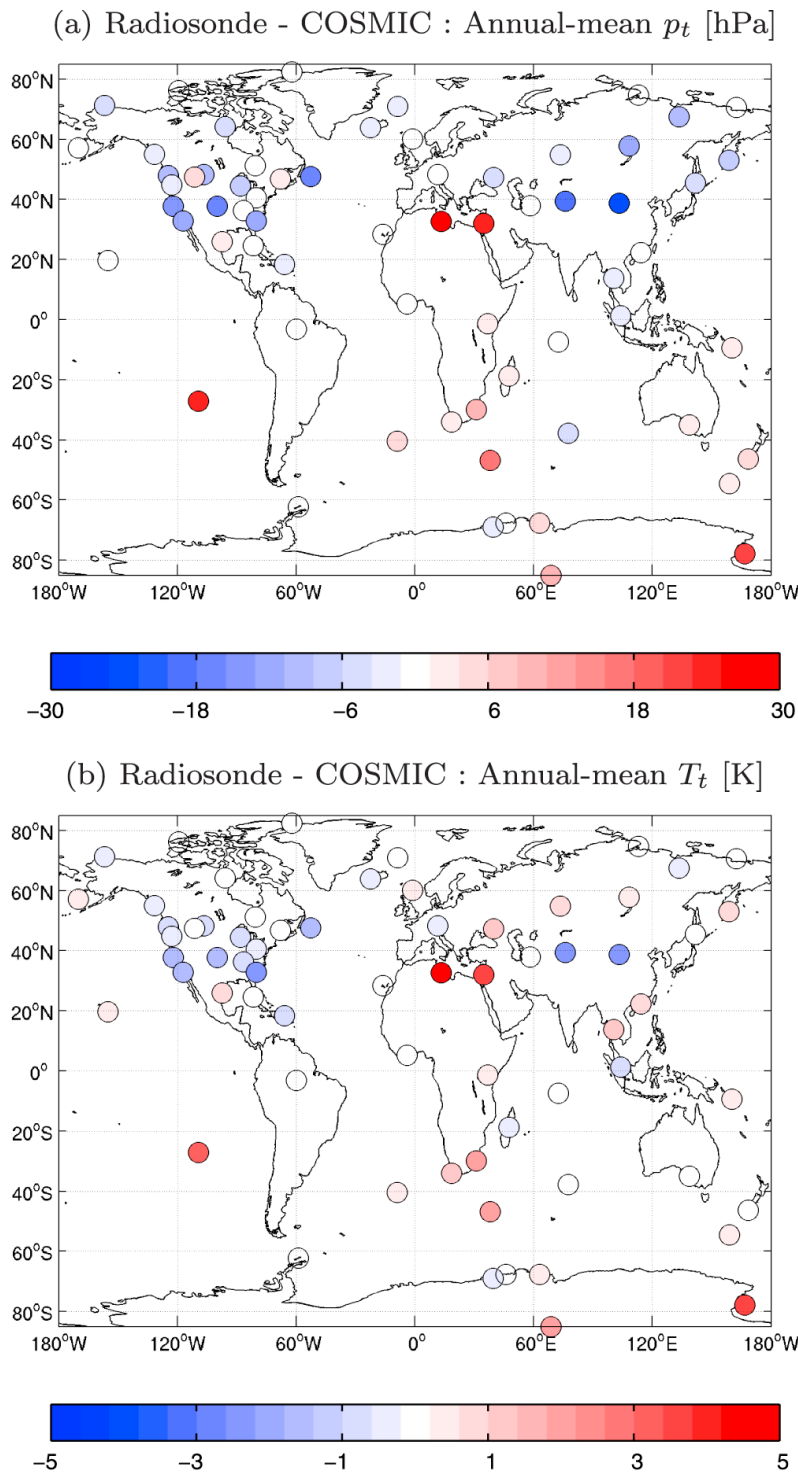## (b) Radiosonde - COSMIC : Annual-mean T_t [K]

Figure 3. Difference of annual mean tropopause properties between radiosonde and COSMIC observations.

all tropopause properties in the Southern Hemisphere (SH) decrease from the midlatitudes (~45°S) to the South Pole. As discussed by *Zängl and Hoinka* [2001], this is largely caused by the stratospheric polar vortex which is colder in the SH than in the NH.

[24] Next we consider the longitudinal structure of tropopause properties. Figures 2a–2c show that all three tropopause properties are largely symmetric in the zonal direction. A considerable asymmetry is found only in the deep tropics and in the NH extratropics. In the tropics, all tropopause properties show extrema in three regions. These regions largely coincide with the regions of strong convection (shading in Figure 2e), and suggest that the spatial distribution of the tropical tropopause is significantly influenced by localized
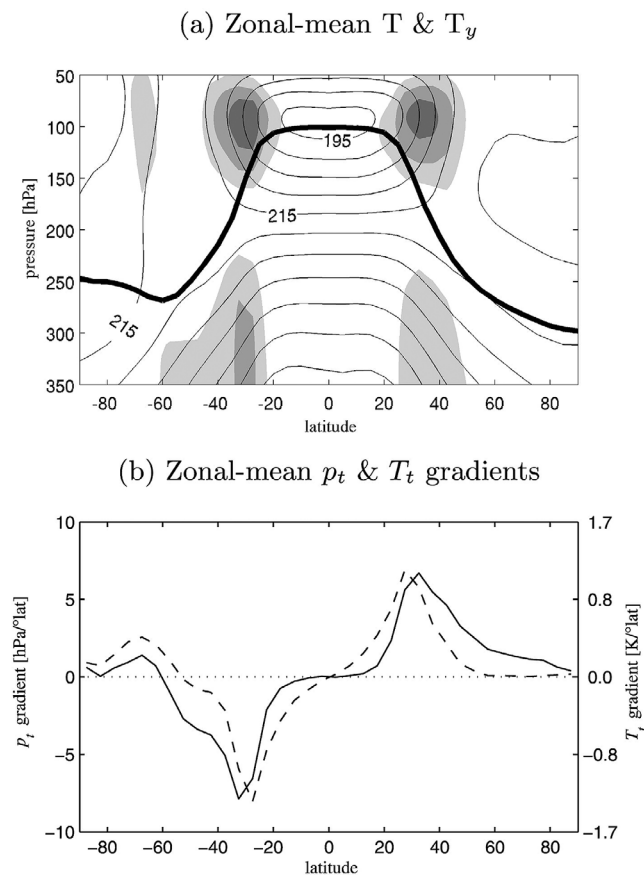
(a) Zonal-mean T & T_y

(b) Zonal-mean p_t & T_t gradients

Figure 4. (a) Annual mean zonal mean temperature (contours) and its latitudinal gradient (shading) and (b) latitudinal gradient of p_t (solid line) and T_t (dashed line) derived from COSMIC observations. The thick line in Figure 4a denotes the climatological tropopause pressure.

deep convection and related UTLS processes [*Highwood and Hoskins*, 1998; *Seidel et al.*, 2001]. In the NH extratropics, p_t exhibits maxima around 70°W and 150°E. These two local maxima reflect an influence of stationary waves (Figure 2e). For instance the maximum p_t over northeastern Canada and western Greenland is collocated with a negative geopotential height anomaly at 500 hPa.

[25] It is noteworthy that while the spatial distribution of T_t is qualitatively similar to that of p_t in the NH, the regions of maximum T_t are more zonally elongated over the northeastern Pacific and North Atlantic. This elongation is partly due to the storm tracks. *Son et al.* [2007] have shown that transient eddies tend to increase T_t on the poleward side of the storm track. Consistent with their findings, the regions of maximum T_t are located on the poleward side of the storm tracks (shading in Figure 2d). No storm track signal is, however, found in the annual mean NH N_t^2 (Figure 2c). This does not imply that N_t^2 is insensitive to storm track eddies: in fact, it simply results from the strong cancellation between warm and cold seasons, as shown in section 3.2.

3.2. Seasonal Cycle

[26] Figure 5 presents the seasonal mean tropopause properties during DJF and JJA. They are again quite similar to the ones derived from the coarser resolution GPS RO

observations [e.g., *Schmidt et al.*, 2005] but show much richer structure. Since p_t and T_t share qualitatively similar features, we first discuss them. The characteristics of N_t^2 are then discussed separately.

[27] The tropical p_t and T_t exhibit a relatively weak seasonality (Figures 5a, 5b, 5d, and 5e). Maximum differences between DJF and JJA are only about 10 hPa in p_t and 10 K in T_t, much smaller than those in the extratropics. But the tropics still show a clear seasonal contrast: the nonzonal feature in the boreal winter disappears in the summer. This indicates that the longitudinal structure evident in the climatological tropopause properties (Figures 2a and 2b) is mostly due to boreal winter conditions. Convection alone does not appear to account for this behavior. Climatological OLR exhibits localized maxima over Africa, Southeast Asia and Central America year round, but the tropopause properties show little sensitivity to this in JJA. Even in DJF, the locations of deep convection and the minima of T_t and p_t do not match exactly: the p_t and T_t minima are located at the equator although OLR minima are located around 10°S. This suggests that the tropical tropopause is not solely controlled by localized deep convection. Other processes, such as convectively driven waves, may also play a role in setting the tropical tropopause [*Highwood and Hoskins*, 1998].

[28] In the extratropics, tropopause properties show a significant zonal asymmetry in NH DJF. This nonzonal structure is largely due to the stationary waves and storm track activity (Figures 5a–5c), and essentially disappears during JJA (Figures 5d–5f). This again indicates that the longitudinal structure of the climatological tropopause properties, shown in Figures 2a and 2b, results largely from boreal winter conditions. From this, one may expect that the seasonal cycle of the extratropical tropopause is primarily controlled by stationary waves and the storm tracks. While this is partly true in the midlatitudes, it appears not to be the case in the high latitudes. For instance, the high-latitude T_t is lower than the midlatitude T_t in cold seasons in both hemispheres. Furthermore, the high-latitude tropopause in the SH, where stationary waves and storm tracks are relatively weak, has a stronger seasonality than in the NH. This strong seasonality in the high latitudes is instead associated with the stratospheric polar vortex. *Zängl and Hoinka* [2001] showed that extremely cold air extending downward from the stratosphere can cause p_t and T_t to decrease in the polar regions in cold seasons. The colder T_t in the SH than in the NH high latitudes also simply results from the greater strength and stability of the Antarctic polar vortex compared to the Arctic vortex. This suggests that the seasonal cycle of the extratropical tropopause is more sensitive to stratospheric processes than tropospheric processes.

[29] Figures 5c–5f present the N_t^2 distribution during DJF and JJA. N_t^2 undergoes a strong seasonal cycle (compare Figures 2c, 5c, and 5f). Although not shown, overall spatial structure of N_t^2 is remarkably similar to N_{LS}^2 distribution [see *Grise et al.*, 2010, Figure 6], suggesting that N_t^2 is dominated by N_{LS}^2. It is again found that, while the spatial structure and seasonality of N_t^2 are negatively correlated with those of T_t in the tropics (compare Figures 5a and 5e with Figures 5c and 5f), they are not well matched in the extratropics. For instance, subtropical maxima in T_t, especially those over the Tibetan plateau during JJA, are absent in N_t^2. Maximum N_t^2 is simply observed in the storm track regions where synoptic-scale
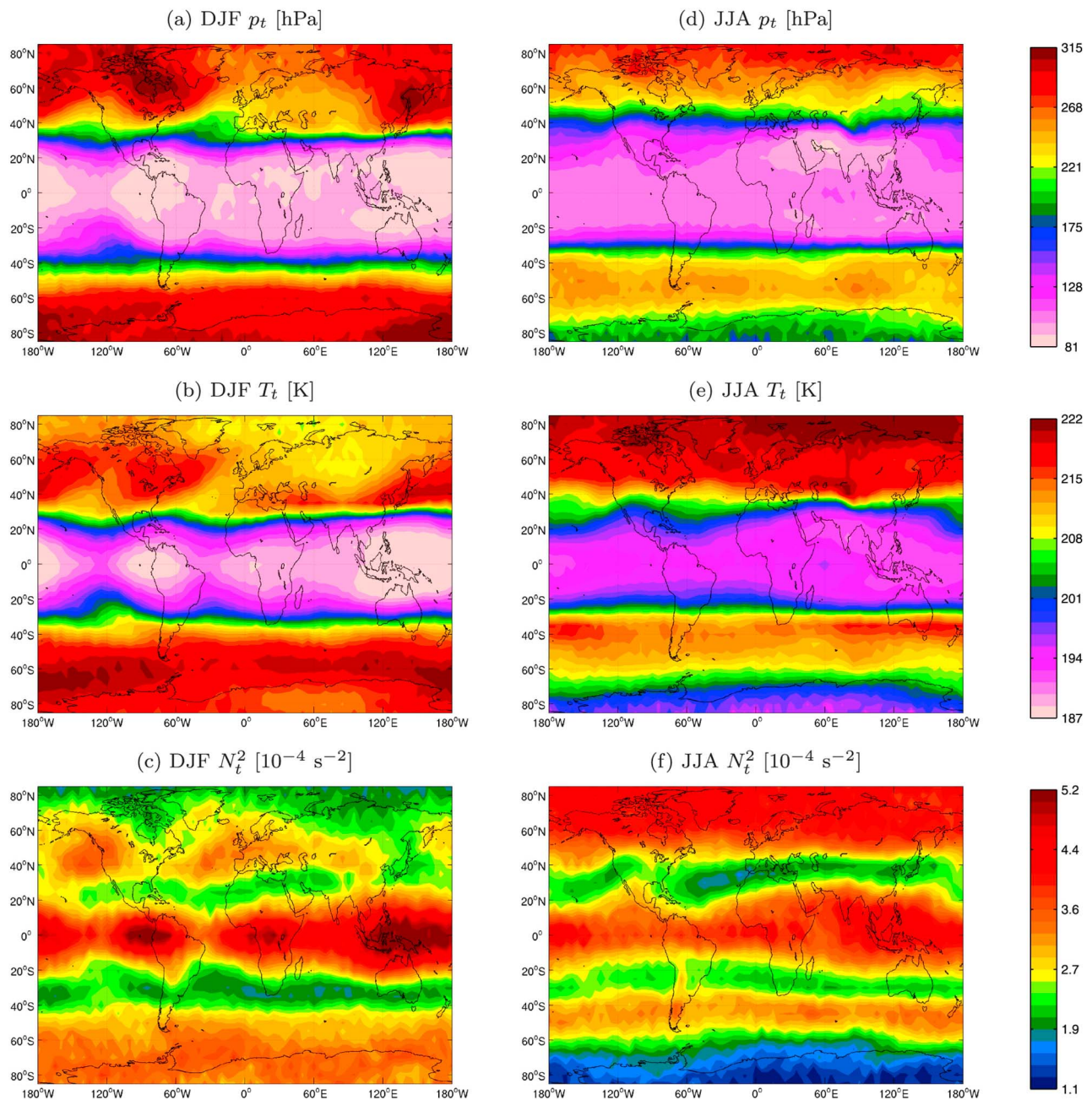
Figure 5. Seasonal mean tropopause properties for (a–c) DJF and (d–f) JJA.

weather systems are active. This result suggests that midlatitude N_t^2 is strongly constrained by baroclinic eddies, supporting the hypothesis that midlatitude TIL is primarily driven by tropospheric dynamics [*Wirth*, 2003] although other processes [e.g., *Birner*, 2010b; *Randel and Wu*, 2010] might still contribute.

[30] It is evident from Figures 5c and 5f that the seasonal cycle of extratropical N_t^2 is not solely controlled by storm track eddies. In fact, as with p_t and T_t, N_t^2 shows the strongest seasonality in the high latitudes. In both hemispheres, the polar summer (winter) exhibits maximum (minimum) N_t^2 (Figures 5c and 5f). *Randel et al.* [2007a], *Kunz et al.* [2009] and *Randel and Wu* [2010] have related these summertime maxima in high-latitude N_t^2 to the water vapor concentration in the UTLS. Water vapor concentrations near the polar tropopause reach their maximum during the summer because of warmer tropospheric temperatures. This increased water vapor causes radiative cooling near the tropopause, generating a strong temperature inversion layer right above the tropopause. *Randel and Wu* [2010] further argued that this radiative process can also explain the hemispheric difference in high-latitude N_t^2: the Arctic N_t^2 is higher than the Antarctic N_t^2 during the summer (compare Figures 5c and 5f) as water vapor concentrations near the tropopause are higher in the Arctic than in the Antarctic.

[31] Since tropopause properties are, to a first order, uniform in the zonal direction (except in the deep tropics and NH
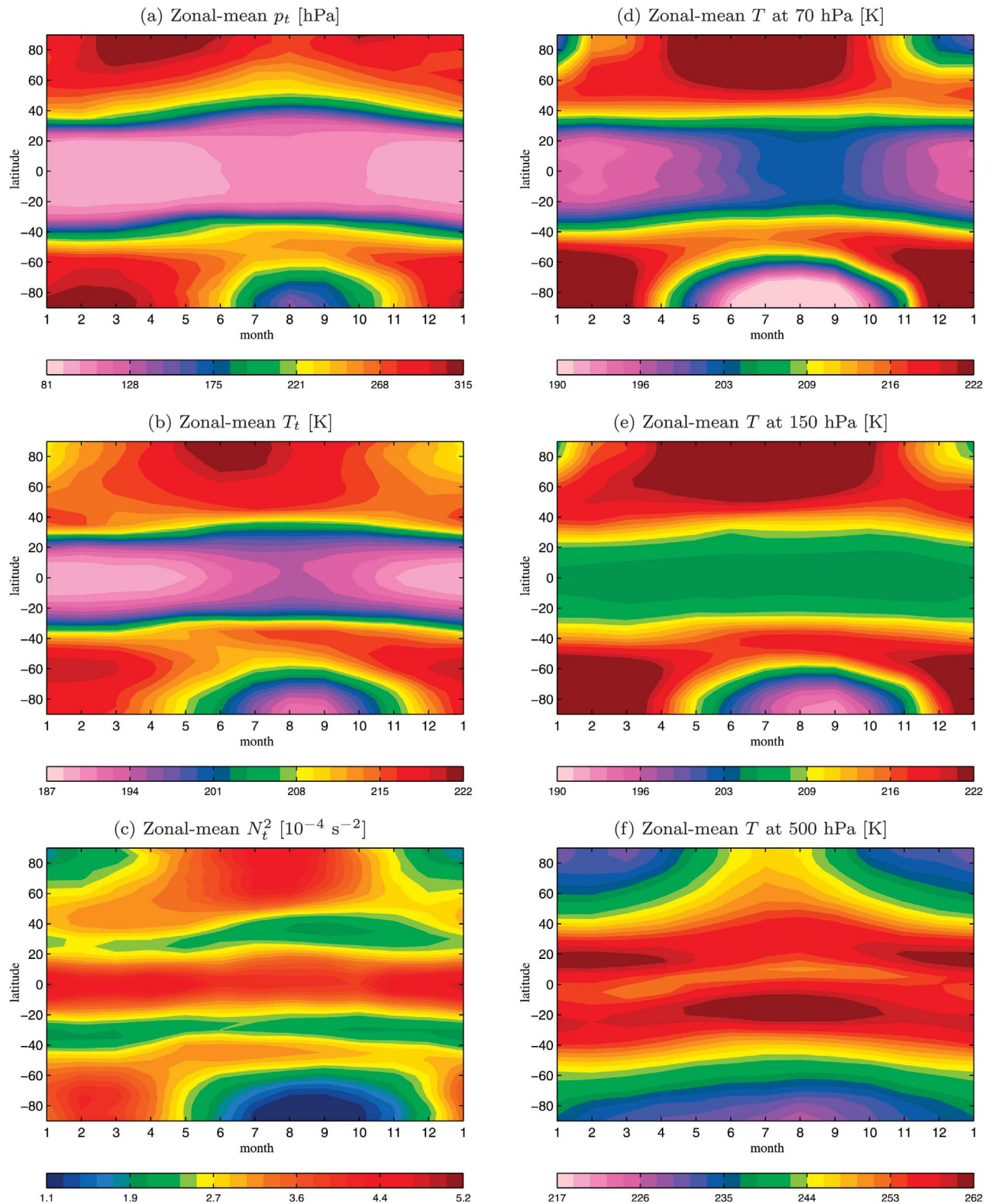
Figure 6. Monthly evolution of (a–c) zonal mean tropopause properties and (d–f) zonal mean temperature at 70, 150, and 500 hPa.

extratropics during DJF), it is informative to look at the seasonal evolution of the zonal mean tropopause properties (Figures 6a–6c). In the tropics both p_t and T_t show minimum values in the boreal winter. They gradually increase until August then decrease (Figures 6a and 6b). This is consistent with the seasonality of tropical upwelling driven by the Brewer-Dobson circulation [e.g., *Yulaeva et al.*, 1994; *Randel et al.*, 2002]. Previous studies have shown that strong

upwelling during the boreal winter tends to push the tropopause height upward, lowering both p_t and T_t [*Reid and Gage*, 1996; *Highwood and Hoskins*, 1998; *Randel et al.*, 2000]. This suggests that, while the longitudinal structure of the tropical tropopause properties is largely controlled by localized deep convection and the related UTLS processes, the zonal mean properties and their seasonal cycles are primarily determined by stratospheric processes as proposed by *Highwood and Hoskins* [1998] and *Seidel et al.* [2001].

[32] In the extratropics, tropopause properties generally reach their maxima in the warm season and minima in the cold season. One exception is p_t in the Arctic, which shows a primary maximum in April and a secondary maximum in October (Figure 6a). This is not an artifact of sampling errors, as similar results are also found in radiosonde [*Highwood et al.*, 2000] and reanalysis data [*Zängl and Hoinka*, 2001]. Although not fully understood, this behavior shows partial correspondence to the Brewer-Dobson circulation. It is well known that high-latitude downwelling reaches its maximum intensity in March–April, a few months later than the maximum upwelling in the deep tropics [e.g., *Appenzeller et al.*, 1996; *Randel et al.*, 2002]. As discussed in the work of *Highwood et al.* [2000], this likely pushes the polar tropopause height downward, increasing p_t. It however remains unclear why Arctic p_t behaves so differently from T_t (compare Figures 6a and 6b), and what causes the secondary maximum of p_t in October. Although there is no reason to expect a linear relationship between p_t and T_t, this puzzling relationship between Arctic p_t and T_t, which does not occur in the Antarctic, deserves further analysis.

[33] The seasonal cycle of N_t^2 is qualitatively similar to that of T_t except in subtropical minima (Figures 6b and 6c). However they are not exactly matched. In particular, the maximum N_t^2 in the polar regions is delayed by about a month compared to the maximum T_t. In the Arctic, the maximum N_t^2 is found in July–August, whereas maximum T_t occurs in June–July. Similarly in the Antarctic, maximum N_t^2 is observed in February–March, about a month after the T_t maximum. This delay has again a closer correspondence to water vapor concentrations as shown by *Randel and Wu* [2010, Figures 9a and 13a].

[34] In order to identify the relative importance of UT and LS processes in the seasonal march of the zonal mean tropopause properties, the seasonal cycle of T_t (Figure 6b) is further compared with that of temperature at three pressure levels: 70, 150 and 500 hPa (Figures 6d–6f). These three levels are chosen to represent temperature in the tropical LS, the tropical UT and extratropical LS, and the extratropical UT, respectively. In the tropics, the seasonal cycle of T_t closely resembles that of LS temperature (compare Figures 6b and 6d). Even in the extratropics, T_t evolves in accordance with LS temperature although tropospheric processes are nonnegligible in the NH midlatitudes (e.g., maximum T_t in July–August around 45°N) and in the polar regions (e.g., minimum T_t in August at the South Pole). This, once more, suggests that the seasonal cycle of the global tropopause is strongly influenced by stratospheric processes.

3.3. Intraseasonal Variability

[35] The intraseasonal variability of each tropopause property is defined by means of the standard deviation, σ.

Submonthly anomalies are first defined by subtracting instantaneous tropopause properties from their monthly mean value in a given month; they are then squared and averaged for each month. The resulting variance is square-rooted to obtain σ. This approach, which differs from conventional method based on daily climatology, is introduced here because COSMIC GPS radio occultations typically occur less than once a day within each grid box (see Figure 1). In many grid boxes in the tropics and high latitudes, occultations occur only once or never in each calendar day for 3 years. This leaves many missing data and makes daily climatology impossible to be defined. To test the robustness of σ, a similar analysis is also performed by defining anomalies with respect to the seasonal mean value. The results are found to be qualitatively similar to the ones presented in this section (not shown).

[36] Figure 7 shows intraseasonal variabilities of all three tropopause properties for the two seasons. While $\sigma(p_t)$ and $\sigma(T_t)$ have qualitatively similar structures, $\sigma(N_t^2)$ again stands apart. Given this contrast, we first discuss $\sigma(p_t)$ and $\sigma(T_t)$. In the tropics, both $\sigma(p_t)$ and $\sigma(T_t)$ exhibit small amplitude and strong homogeneity (Figures 7a, 7b, 7d, and 7e). Although a weak hint of a local maximum is observed in $\sigma(T_t)$ over the western Pacific (Figure 7b), localized $\sigma(T_t)$ is generally not found over the three regions of strong convection (Figure 2e). This result suggests, surprisingly, that the short-term variability of the tropical tropopause is not directly linked to deep convection. This contrasts with the climatological tropical tropopause, which is largely controlled by deep convection and the related UTLS processes.

[37] In the extratropics, $\sigma(p_t)$ and $\sigma(T_t)$ are relatively strong. The maximum variability is found primarily in the subtropics year-round and over the Tibetan plateau during JJA. Although localized maxima are also found over the storm track regions, they are relatively weaker than the ones in the subtropics. The subtropical maxima largely result from the frequent occurrence of double tropopauses in these regions. Figure 8a presents the probability density function (pdf) of p_t during DJF over subtropical Asia, covering $25°N \leq \phi \leq 35°N$ and $60°E \leq \lambda \leq 120°E$. The pdf shows a distinct bimodal distribution with one peak around 100 hPa, tropical p_t values, and the other peak around 250 hPa, extratropical p_t values (see Figure 8d for individual temperature profiles). Together with $\sigma(p_t)$ shown in Figure 7, this depicts a tropopause that is switching between tropical and extratropical values on intraseasonal time scales. During JJA, extremely high values of $\sigma(p_t)$ and $\sigma(T_t)$ are also observed over the Tibetan plateau. The pdf of p_t and instantaneous temperature profiles are displayed in Figures 8b and 8e. As in Figure 8a, a bimodality of p_t is evident, but, in contrast, the secondary peak is not well defined. Instead, there is a relatively high occurrence of tropopauses around 300–350 hPa that serve to flatten the overall p_t distribution (Figure 8b). The lack of a secondary peak is associated with temperature inversion layers around 350 hPa (Figure 8e). Although detailed analyses are needed, these inversion layers are likely caused by elevated heating as well as monsoon convection over the Tibetan plateau.

[38] Figures 7a and 7d also show that $\sigma(p_t)$ is high over the winter pole, especially in the SH. This is not likely caused by the polar vortex as the vortex is very stable in the SH. As discussed by *Highwood et al.* [2000] and *Zängl and Hoinka*
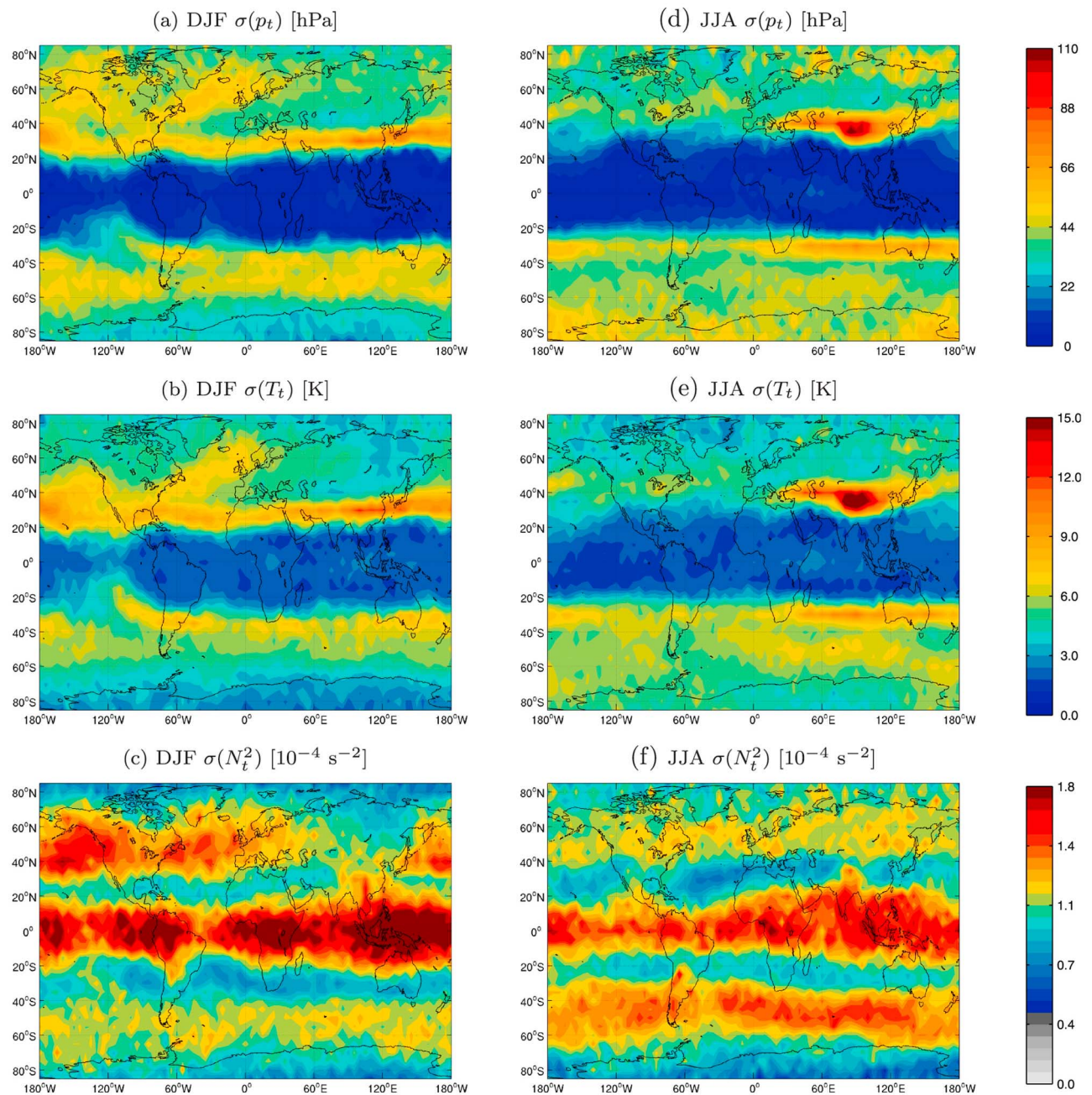
Figure 7. Same as Figure 5 but for intraseasonal variability.

[2001], this is likely caused by the fact that the polar tropopause is not well defined during the cold seasons. Figures 8c and 8f present the pdf of p_t and individual temperature profiles over 70°S poleward during the austral winter. Many profiles have no temperature inversion: temperatures keep decreasing with height well into the stratosphere.

[39] Unlike $\sigma(p_t)$ and $\sigma(T_t)$, the latitude-longitude structure of $\sigma(N_t^2)$ is somewhat similar to that of the climatological N_t^2 (compare Figures 7c and 7f with Figures 5c and 5f). In other words, $\sigma(N_t^2)$ is strong in the tropics and storm track regions but negligible in the subtropics. A notable exception is found in the summer hemisphere high latitudes: $\sigma(N_t^2)$ shows

negligible values where the climatological N_t^2 is maximum. Since the short-term variability associated with radiative processes is typically weaker than the one with dynamical processes in the LS, this result supports the hypothesis of a radiative (rather than dynamical) formation of the TIL in the high latitudes [*Randel et al.*, 2007a; *Kunz et al.*, 2009; *Randel and Wu*, 2010]. It is also noteworthy that $\sigma(N_t^2)$ is maximum in the tropics where $\sigma(T_t)$ is minimum. A preliminary analysis has revealed that this is at least in part caused by equatorial waves which propagate vertically [*Son and Lee*, 2007; *Ryu et al.*, 2008]. *Son and Lee* [2007], for example, showed that temperature in the tropical UTLS is significantly modulated
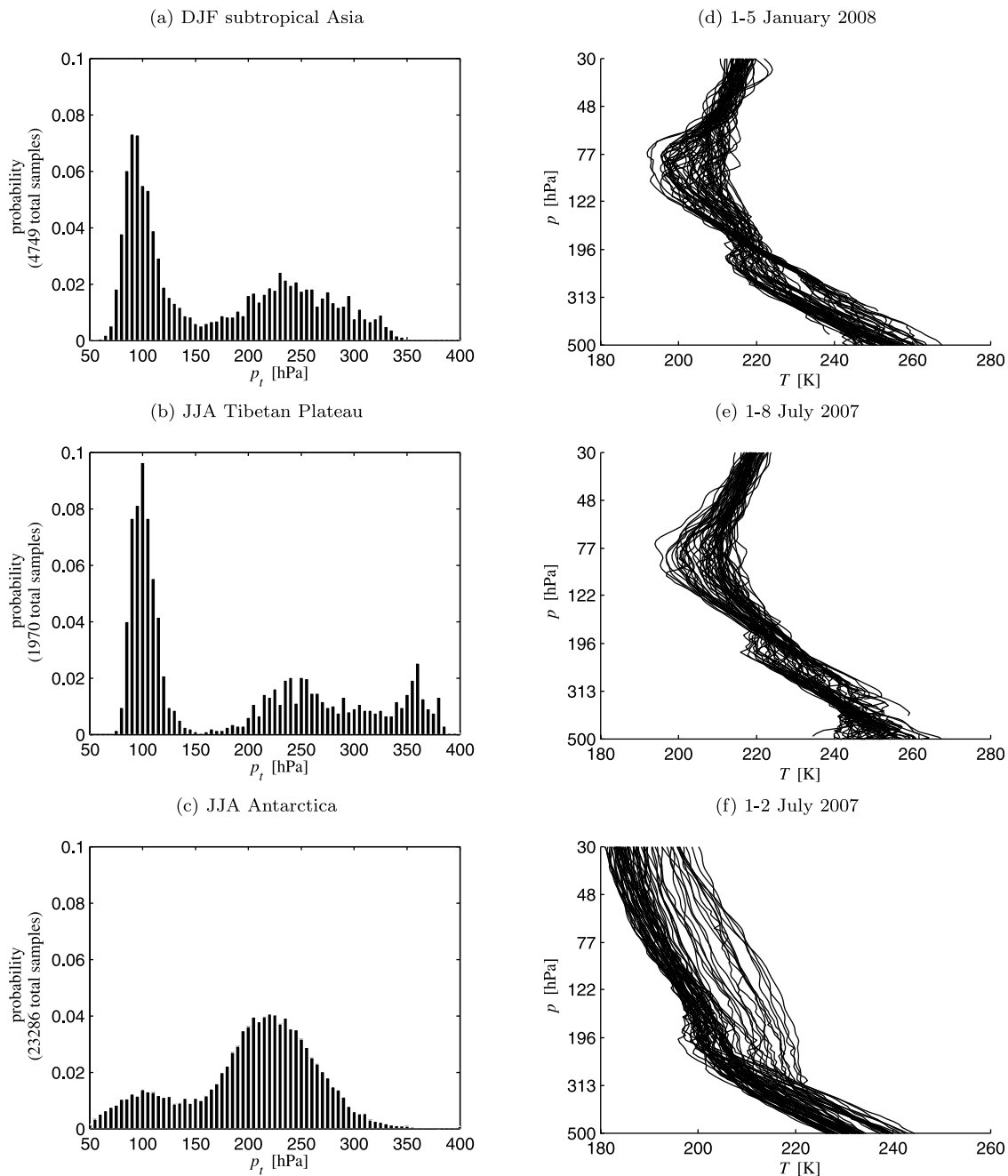
Figure 8. (a–c) The pdfs of p_t and (d–f) vertical temperature profiles from three regions: subtropical Asia over 25°N–35°N and 60°E–120°E during boreal winter (Figures 8a and 8d), Tibetan plateau over 34°N–44°N and 72°E–100°E during boreal summer (Figures 8b and 8e), and Antarctica over 70°S–90°S during austral winter (Figures 8c and 8f). For clarity, temperature profiles include only a subset of soundings, as indicated in each plot.

by convectively driven waves, particularly those associated with the Madden-Julian Oscillation on intraseasonal time scales. Details of this will be presented in a separate paper.

[40] Finally, the seasonal cycle of intraseasonal variability is examined with zonal mean $\sigma(p_t)$, $\sigma(T_t)$, and $\sigma(N_t^2)$ in Figure 9. Consistent with Figure 7, both $\sigma(p_t)$ and $\sigma(T_t)$ exhibit weak seasonality in the deep tropics. In the extratropics, both $\sigma(p_t)$ and $\sigma(T_t)$ show strong intraseasonal variability around the subtropical jet, where double tropopauses frequently occur. Strong variability is also evident in the SH high latitudes in July when the tropopause is not well defined. However, the intraseasonal variability associated with extratropical storm tracks does not stand out in the zonal mean fields. This result contrasts $\sigma(N_t^2)$ which shows strong seasonality in the midlatitudes only. Although $\sigma(N_t^2)$ shows maximum values in the tropics, its seasonal cycle is relatively weak. This suggests that extra-
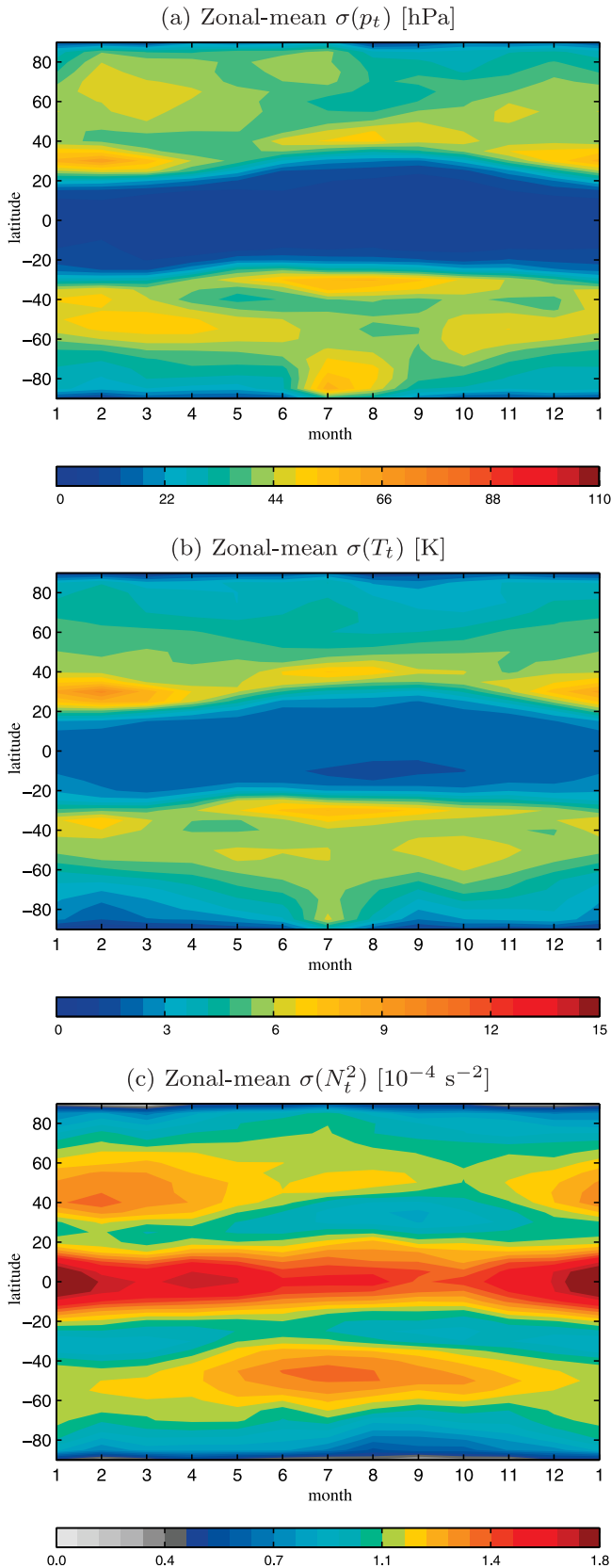
(a) Zonal-mean $\sigma(p_t)$ [hPa]

(b) Zonal-mean $\sigma(T_t)$ [K]

(c) Zonal-mean $\sigma(N_t^2)$ [10^{-4} s^{-2}]

Figure 9.   Same as Figure 6 but for intraseasonal variability.

tropical storm tracks effectively modulate the vertical temperature gradient near the tropopause.

[41] From Figures 7 and 9, it might be concluded that the polar tropopause is relatively stable on intraseasonal time scales, especially in the Arctic. This is, however, not true during the boreal winter. As shown in the work of *Zängl and Hoinka* [2001] and *Grise et al.* [2010], Arctic tropopause properties can abruptly change as the stratospheric polar vortex suddenly breaks down. Such events, which are often referred to as sudden stratospheric warming (SSW) events, occurred once in the analysis period. Figure 10a shows time series of polar cap temperature at 50 hPa averaged over 60°N to the North Pole. In January 2009, polar cap temperature increases sharply by about 20 K in 10 days [see also *Martineau and Son*, 2010, Figure 3]. This temperature change is much larger than any short-term temperature changes observed during 2007 and 2008 boreal winters.

[42] The impact of the 2009 SSW event on Arctic tropopause properties is illustrated in Figures 10b–10d. Both p_t and T_t abruptly increase (e.g., about 7 K warming of T_t and 60 hPa increase of p_t in 10 days) and maintain their values for over a month (see thick black lines). Although the response of N_t^2 is somewhat noisy, it also shows an increase with a time lag. This result suggests that SSW events can effectively modulate Arctic tropopause properties, confirming previous studies [*Zängl and Hoinka*, 2001; *Grise et al.*, 2010]. Given this evidence, it is puzzling why Figures 7 and 9 do not show strong $\sigma(p_t)$ and $\sigma(T_t)$ in the NH high latitudes during the boreal winter. This can be explained by the infrequent occurrence of SSW events, i.e., only one event in the analysis period.

4.   Evaluation of NNR Tropopause Data

[43] As described in section 1, tropopause properties have been widely used in climate studies. Such studies have primarily relied on reanalysis data because of their global coverage over a long-term period. Among reanalysis data sets, NNR data have been particularly popular as p_t and T_t are directly available. The quality of NNR tropopause data, however, has rarely been evaluated using high-resolution observations. Although a couple of studies have examined tropical tropopause properties of NNR data [e.g., *Randel et al.*, 2000], quantitative evaluation of NNR tropopause data over the whole globe has not been conducted. In order to provide helpful guidance or possibly a cautionary note on NNR tropopause data, this section briefly evaluates NNR tropopause data by comparing them with COSMIC observations.

[44] Figures 11a and 11c present the differences of seasonal mean p_t between COSMIC and NNR data. These are generated by simply subtracting seasonal mean values. Significant biases, up to ~60 hPa, are found in the subtropics and high latitudes with a maximum negative bias over the Tibetan plateau during JJA. Although not shown, similar results are also found in T_t where the bias ranges from −20 to 20 K. These biases are much larger than those reported in the literature. For instance, by comparing the tropopause properties derived from CHAMP and SAC-C data with those from ECMWF operational analysis data, *Schmidt et al.* [2005] have shown that the differences in tropopause properties between GPS RO observations and analysis data are typically less than
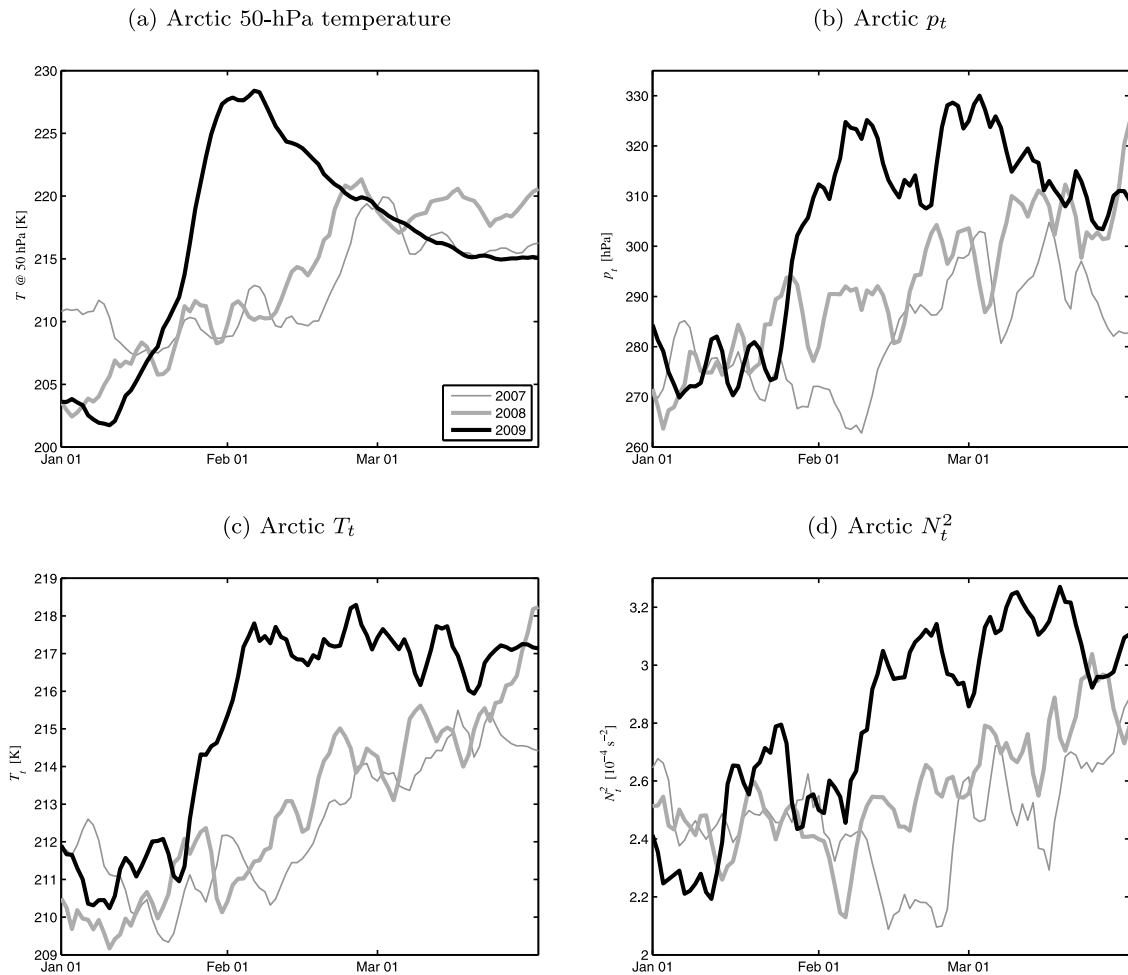
(a) Arctic 50-hPa temperature   (b) Arctic p_t

(c) Arctic T_t (d) Arctic N_t^2

Figure 10. Time evolution of the Arctic tropopause properties taken using a cosine-weighted 3 day average from 60°N to the North Pole. Only January to March are shown for each of the 3 years.

10 hPa in p_t and 3 K in T_t in both hemispheres [see *Schmidt et al.*, Figure 10].

[45] The bias of NNR p_t data is further quantified by using $\sigma(p_t)$ (Figures 11b and 11d). It is again found that NNR p_t data severely underestimate intraseasonal variability of p_t (and T_t) in almost all locations except in the NH extratropics during DJF where $\sigma(p_t)$ is slightly overestimated in several regions (Figure 11b). The underestimate is particularly large in the subtropics and exhibits a maximum over the Tibetan plateau during JJA. Although not shown, strong p_t variability over the Tibetan plateau (Figure 7d) is essentially absent in NNR p_t data.

[46] These results suggest that NNR tropopause data have significant and systematic biases, and should be used with great caution in any quantitative studies. The preliminary analyses show that the biases are likely introduced by relative coarse vertical resolution of NNR and lack of observations especially in the SH. The biases might also be partly caused by an inaccurate tropopause detection algorithm used by NNR. By comparing tropopause properties directly available from NNR and those independently computed from model-level NNR temperature data with more precise algorithm, *Birner* [2010a] found significant differences between the two

in the subtropics [see *Birner*, 2010a, section 2]. More detailed analyses and investigation of other reanalysis data sets will be presented in a future study.

5. Summary and Discussion

[47] We have examined the spatiotemporal structure of the global tropopause using state-of-the-art GPS RO measurements from the COSMIC mission [*Anthes et al.*, 2008]. The climatology, seasonal cycle and intraseasonal variability were analyzed for three tropopause properties: lapse-rate tropopause pressure (p_t), temperature (T_t) and sharpness (N_t^2). The overall results are qualitatively similar to the previous studies which are based on reanalyses [*Hoerling et al.*, 1991; *Hoinka*, 1998, 1999; *Highwood et al.*, 2000; *Zängl and Hoinka*, 2001], radiosonde [*Reid and Gage*, 1996; *Seidel et al.*, 2001; *Seidel and Randel*, 2006] and earlier GPS RO data [*Schmidt et al.*, 2005; *Grise et al.*, 2010]. It is however found that NNR tropopause data, which are directly available from the NNR Web site, have significant and systematic biases, suggesting that they should be used with great caution in quantitative studies. Key findings of COSMIC data analysis are summarized below.
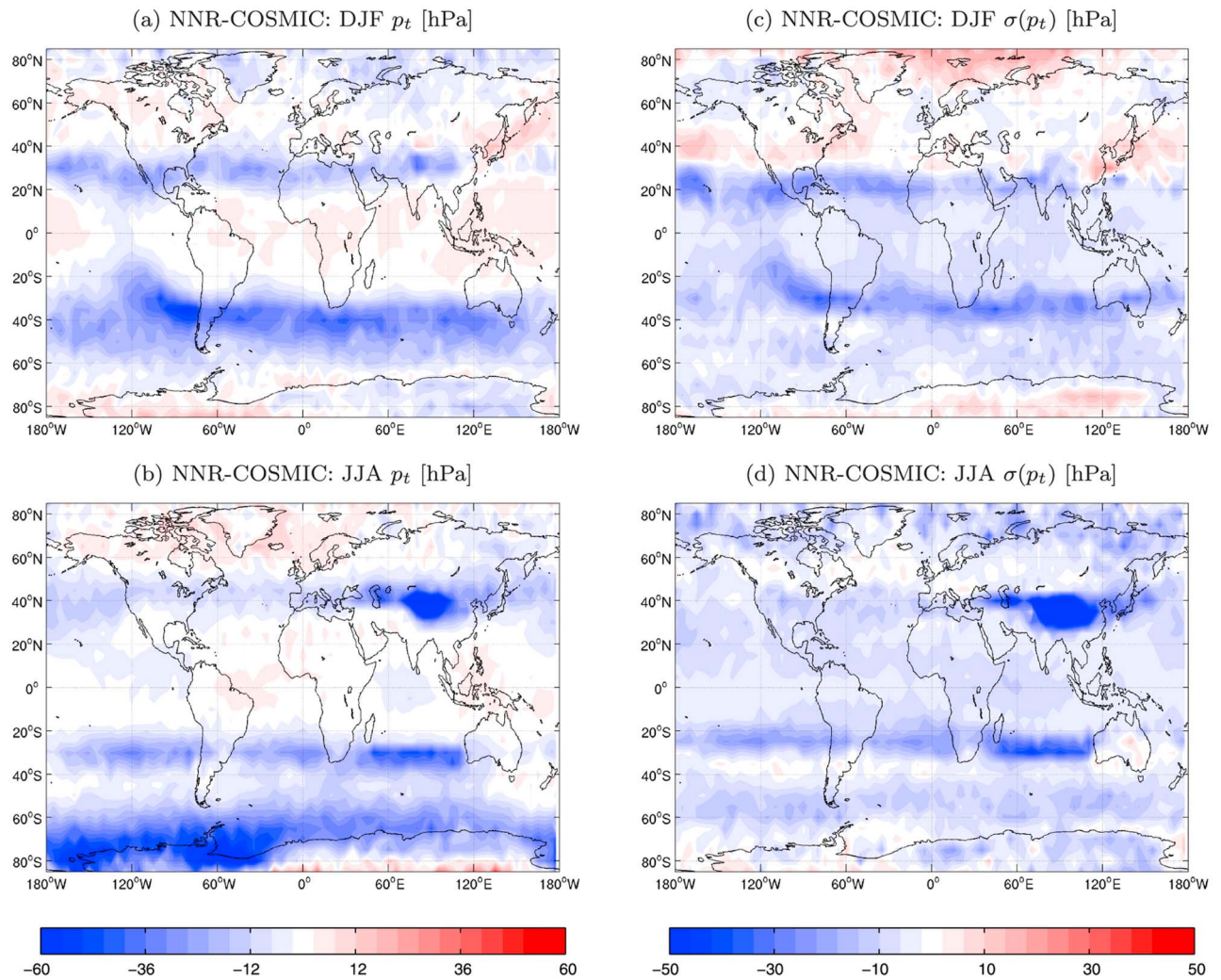
Figure 11. Seasonal mean (a and b) p_t and (c and d) $\sigma(p_t)$ differences between NNR and COSMIC for DJF (a and c) and JJA (b and d).

[48] Climatological tropopause properties are largely homogeneous in the zonal direction. Longitudinal variations are found only in the deep tropics and in the NH extratropics during the boreal winter. These are associated with localized deep convection and related UTLS processes (e.g., convectively driven waves) in the tropics, and with stationary waves and storm track activity in the NH. All tropopause properties show a stronger seasonal cycle in the high latitudes than in the tropics, with maximum variability at the poles. In the tropics, p_t and T_t are generally lowest in December and highest in August. N_t^2 simply follows T_t, with an out-of-phase relationship. In the extratropics, all tropopause properties have a minimum in the cold season in both hemispheres. This seasonality is largely explained by the Brewer-Dobson circulation, the polar vortex and the radiative processes in the UTLS.

[49] The intraseasonal variability of tropopause properties, one of the novel aspects of this study, shows very rich structure. Both p_t and T_t show significant variability in the subtropics along the subtropical jet in both hemispheres, the storm track regions in the winter hemisphere, the Tibetan plateau in JJA,

and the pole in the winter hemisphere. Their variabilities are, however, minimum and zonally homogeneous in the deep tropics, suggesting that tropical deep convection plays only a minor role there. The intraseasonal variability of N_t^2 drastically differs from that of p_t and T_t: it has maximum values in the tropics, where p_t and T_t have minimum variability. In the extratropics, N_t^2 has significant variability only in the storm track regions with minimum variability in the subtropics.

[50] An important but missing piece of analysis in this study, among others, is interannual variability. With only 3 year long observations used in this study, interannual variability can hardly be examined in quantity. It is however known, from the observations and reanalysis data, that the tropopause properties are significantly modulated by El Niño–Southern Oscillation (ENSO) and stratospheric quasi-biennial oscillation (QBO) in the tropics [e.g., *Randel et al.*, 2000], by stratospheric ozone concentrations in the SH high latitudes [e.g., *Wong and Wang*, 2003], and possibly by SSW events in the NH high latitudes. With longer GPS RO measurements, these can be better quantified.

[51] It should be noted that, while this study helps us better characterize the global tropopause, its physical implication is somewhat limited. In this study, tropopause is defined with temperature lapse rate as it can be easily identified over the globe. It is however well known that the dynamic tropopause is more meaningful in the extratropics than the lapse-rate tropopause. Likewise, in the tropics, the cold-point tropopause is physically more meaningful. The detailed characteristics of these other definitions are currently under investigation. The results are to be presented in a future study.

References

Anthes, R. A., et al. (2008), The COSMIC/FORMOSAT-3 mission: Early results, *Bull. Am. Meteorol. Soc.*, *89*(3), 313–333.

Appenzeller, C., J. R. Holton, and K. H. Rosenlof (1996), Seasonal variation of mass transport across the tropopause, *J. Geophy. Res.*, *101*(D10), 15,071–15,078.

Birner, T. (2006), Fine-scale structure of the extratropical tropopause region, *J. Geophys. Res.*, *111*, D04104, doi:10.1029/2005JD006301.

Birner, T. (2010a), Recent widening of the tropical belt from global tropopause statistics: Sensitivities, *J. Geophys. Res.*, *115*, D23109, doi:10.1029/2010JD014664.

Birner, T. (2010b), Residual circulation and tropopause structure, *J. Atmos. Sci.*, *67*, 2582–2600, doi:10.1175/2010JAS3287.1.

Birner, T., A. Dörnbrack, and U. Schumann (2002), How sharp is the tropopause at midlatitudes?, *Geophys. Res. Lett.*, *29*(14), 1700, doi:10.1029/2002GL015142.

Birner, T., D. Sankey, and T. G. Shepherd (2006), The tropopause inversion layer in models and analyses, *Geophys. Res. Lett.*, *33*, L14804, doi:10.1029/2006GL026549.

Butchart, N., and A. A. Scaife (2001), Removal of chlorofluorocarbons by increased mass exchange between the stratosphere and troposphere in a changing climate, *Nature*, *410*, 799–802.

Durre, I., R. S. Vose, and D. B. Wuertz (2006), Overview of the integrated global radiosonde archive, *J. Clim.*, *19*, 53–68.

Fueglistaler, S., A. E. Dessler, T. J. Dunkerton, I. Folkins, Q. Fu, and P. W. Mote (2009), Tropical tropopause layer, *Rev. Geophys.*, *47*, RG1004, doi:10.1029/2008RG000267.

Gabriel, A., G. Schmitz, and R. Geprägs (1999), The tropopause in a 2D circulation model, *J. Atmos. Sci.*, *56*, 4059–4068.

Grise, K. M., D. W. J. Thompson, and T. Birner (2010), A global survey of static stability in the stratosphere and upper troposphere, *J. Clim.*, *23*, 2275–2292.

He, W., S. Ho, H. Chen, X. Zhou, D. Hunt, and Y.-H. Kuo (2009), Assessment of radiosonde temperature measurements in the upper troposphere and lower stratosphere using COSMIC radio occultation data, *Geophys. Res. Lett.*, *36*, L17807, doi:10.1029/2009GL038712.

Held, I. M. (1982), On the height of the tropopause and the static stability of the troposphere, *J. Atmos. Sci.*, *39*, 412–417.

Highwood, E. J., and B. J. Hoskins (1998), The tropical tropopause, *Q. J. R. Meteorol. Soc.*, *124*, 1579–1604.

Highwood, E. J., B. J. Hoskins, and P. Berrisford (2000), Properties of the Arctic tropopause, *Q. J. R. Meteorol. Soc.*, *126*, 1515–1532.

Hoerling, M. P., T. K. Schaack, and A. J. Lenzen (1991), Global objective tropopause analysis, *Mon. Weather Rev.*, *119*, 1816–1831.

Hoinka, K. P. (1998), Statistics of the global tropopause pressure, *Mon. Weather Rev.*, *126*(12), 3303–3325.

Hoinka, K. P. (1999), Temperature, humidity, and wind at the global tropopause, *Mon. Weather Rev.*, *127*, 2248–2265.

Holton, J. R., P. H. Haynes, M. E. McIntyre, A. R. Douglas, R. B. Rood, and L. Pfister (1995), Stratosphere-troposphere exchange, *Rev. Geophys.*, *33*, 403–440.

Kalnay, E., et al. (1996), The NCEP/NCAR 40-year reanalysis project, *Bull. Am. Meteorol. Soc.*, *77*, 437–472.

Kirk-Davidoff, D. B., and R. S. Lindzen (2000), An energy balance model based on potential vorticity homogenization, *J. Clim.*, *13*, 431–448.

Kishore, P., S. P. Namboothiri, K. Igarashi, J. H. Jiang, C. O. Ao, and L. J. Romans (2006), Climatological characteristics of the tropopause parameters derived from GPS/CHAMP and GPS/SAC-C measurements, *J. Geophys. Res.*, *111*, D20110, doi:10.1029/2005JD006827.

Kunz, A., P. Konopka, R. Müller, L. L. Pan, C. Schiller, and F. Rohrer (2009), High static stability in the mixing layer above the extratropical tropopause, *J. Geophys. Res.*, *114*, D16305, doi:10.1029/2009JD011840.

Kursinski, E. R., G. A. Hajj, S. S. Leroy, and B. Herman (2000), The GPS radio occultation technique, *Terr. Atmos. Ocean. Sci.*, *11*, 53–114.

Liebmann, B., and C. A. Smith (1996), Description of a complete (interpolated) outgoing longwave radiation dataset, *Bull. Am. Meteorol. Soc.*, *77*, 1275–1277.

Lindzen, R. S. (1993), Baroclinic neutrality and the tropopause, *J. Atmos. Sci.*, *50*, 1148–1151.

Lorenz, D. J., and E. T. DeWeaver (2007), Tropopause height and zonal wind response to global warming in the IPCC scenario integrations, *J. Geophys. Res.*, *112*, D10119, doi:10.1029/2006JD008087.

Lu, J. A., G. A. Vecchi, and T. Reichler (2007), Expansion of the Hadley cell under global warming, *Geophys. Res. Lett.*, *34*, L06805, doi:10.1029/2006GL028443.

Manabe, S., and R. F. Strickler (1964), Thermal equilibrium of the atmosphere with a convective adjustment, *J. Atmos. Sci.*, *21*, 361–385.

Martineau, P., and S.-W. Son (2010), Quality of reanalysis data during stratospheric vortex weakening and intensification events, *Geophys. Res. Lett.*, *37*, L22801, doi:10.1029/2010GL045237.

Mote, P. W., K. H. Rosenlof, M. E. McIntyre, E. S. Carr, J. C. Gille, J. R. Holton, J. S. Kinnersley, H. C. Pumphrey, J. M. Russell III, and J. W. Waters (1996), An atmospheric tape recorder: The imprint of tropical tropopause temperatures on stratospheric water vapor, *J. Geophys. Res.*, *101*(D2), 3989–4006, doi:10.1029/95JD03422.

Randel, W. J., and F. Wu (2010), The polar summer tropopause inversion layer, *J. Atmos. Sci.*, *67*, 2572–2581.

Randel, W. J., F. Wu, and D. J. Gaffen (2000), Interannual variability of the tropical tropopause derived from radiosonde data and NCEP reanalyses, *J. Geophys. Res.*, *105*(D12), 15,509–15,523, doi:10.1029/2000JD900155.

Randel, W. J., R. R. Garcia, and F. Wu (2002), Time-dependent upwelling in the tropical lower stratosphere estimated from the zonal-mean momentum budget, *J. Atmos. Sci.*, *59*, 2141–2152.

Randel, W. J., F. Wu, and W. R. Ríos (2003), Thermal variability of the tropical tropopause region derived from GPS/MET observations, *J. Geophys. Res.*, *108*(D1), 4024, doi:10.1029/2002JD002595.

Randel, W. J., F. Wu, and P. Forster (2007a), The extratropical tropopause inversion layer: Global observations with GPS data, and a radiative forcing mechanism, *J. Atmos. Sci.*, *64*, 4489–4496.

Randel, W. J., D. J. Seidel, and L. L. Pan (2007b), Observational characteristics of double tropopauses, *J. Geophys. Res.*, *112*, D07309, doi:10.1029/2006JD007904.

Reid, G. C., and K. S. Gage (1996), The tropical tropopause over the western Pacific: Wave driving, convection, and the annual cycle, *J. Geophys. Res.*, *101*(D16), 21,233–21,241, doi:10.1029/95JD03578.

Ryu, J. H., S. Lee, and S. W. Son (2008), Vertically propagating Kelvin waves and tropical tropopause variability, *J. Atmos. Sci.*, *65*, 1817–1837.

Santer, B. D., et al. (2003a), Contributions of anthropogenic and natural forcing to recent tropopause height changes, *Science*, *301*, 479–483.

Santer, B. D., et al. (2003b), Behavior of tropopause height and atmospheric temperature in models, reanalyses, and observations: Decadal changes, *J. Geophys. Res.*, *108*(D1), 4002, doi:10.1029/2002JD002258.

Schmidt, T., S. Heise, J. Wickert, G. Beyerle, and C. Reigber (2005), GPS radio occultation with CHAMP and SAC-C: Global monitoring of thermal tropopause parameters, *Atmos. Chem. Phys.*, *5*, 1473–1488.

Schneider, T. (2004), The tropopause and the thermal stratification in the extratropics of a dry atmosphere, *J. Atmos. Sci.*, *61*, 1317–1340.

Seidel, D. J., and W. J. Randel (2006), Variability and trends in the global tropopause estimated from radiosonde data, *J. Geophys. Res.*, *111*, D21101, doi:10.1029/2006JD007363.

Seidel, D. J., and W. J. Randel (2007), Recent widening of the tropical belt: Evidence from tropopause observations, *J. Geophys. Res.*, *112*, D20113, doi:10.1029/2007JD008861.

Seidel, D. J., R. Ross, J. K. Angell, and G. C. Reid (2001), Climatological characteristics of the tropical tropopause as revealed by radiosondes, *J. Geophys. Res.*, *106*(D8), 7857–7878, doi:10.1029/2000JD900837.

Son, S.-W., and S. Lee (2007), Intraseasonal variability of the zonal-mean tropical tropopause height, *J. Atmos. Sci.*, *64*, 2695–2706.

Son, S.-W., and L. M. Polvani (2007), Dynamical formation of an extratropical tropopause inversion layer in a relatively simple general circulation model, *Geophys. Res. Lett.*, *34*, L17806, doi:10.1029/2007GL030564.

Son, S.-W., S. Lee, and S. B. Feldstein (2007), Intraseasonal variability of the zonal-mean extratropical tropopause height, *J. Atmos. Sci.*, *64*, 608–620.

Son, S.-W., L. M. Polvani, D. W. Waugh, T. Birner, H. Akiyoshi, R. R. Garcia, A. Gettelman, D. A. Plummer, and E. Rozanov (2009), The impact of stratospheric ozone recovery on tropopause height trends, *J. Clim.*, *22*, 429–445.

Thuburn, J., and G. G. Craig (2000), Stratospheric influence on tropopause height: The radiative constraint, *J. Atmos. Sci.*, *57*, 17–28.

Wirth, V. (2003), Static stability in the extratropical tropopause region, *J. Atmos. Sci.*, *60*, 1395–1409.

Wong, S., and W.-C. Wang (2003), Tropical-extratropical connection in interannual variation of the tropopause: Comparison between NCEP/NCAR reanalysis and an atmospheric general circulation model simulation, *J. Geophys. Res.*, *108*(D2), 4043, doi:10.1029/2001JD002016.

World Meteorological Organization (WMO) (1957), Meteorology: A three-dimensional science, *WMO Bull.*, *4*, pp. 134–138, Geneva, Switzerland.

Yulaeva, E., J. R. Holton, and J. M. Wallace (1994), On the cause of the annual cycle in tropical lower-stratospheric temperatures, *J. Atmos. Sci.*, *51*, 169–174.

Zängl, G., and K. P. Hoinka (2001), The tropopause in the polar regions, *J. Clim.*, *14*, 3117–3139.

Zängl, G., and V. Wirth (2002), Synoptic-scale variability of the polar and subpolar tropopause: Data analysis and idealized PV inversions, *Q. J. R. Meteorol. Soc.*, *128*, 2301–2315.

L. M. Polvani and N. F. Tandon, Department of Applied Physics and Applied Mathematics, Columbia University, 500 W. 120th St., New York, NY 10027, USA.

S.-W. Son, Department of Atmospheric and Oceanic Sciences, McGill University, 805 Sherbrooke St. W., Montreal, QC H3A 2K6, Canada. (seok-woo.son@mcgill.ca)